Applied Thermal Engineering 31 (2011) 3971–3978

Contents lists available at ScienceDirect

Applied Thermal Engineering

journal homepage: www.elsevier.com/locate/apthermeng

# Improvement of passive fire protection in a gypsum panel by adding inorganic fillers: Experiment and theory

Aleix Ciudad [a,*], A.M. Lacasta [a], L. Haurie [b], J. Formosa [a,c], J.M. Chimenos [c]

[a] Departament de Física Aplicada, Universitat Politècnica de Catalunya, Av.Dr. Marañón 44, E-08028 Barcelona, Spain
[b] Departament de Construccions Arquitectòniques II, Universitat Politècnica de Catalunya, Av.Dr. Marañón 44, E-08028 Barcelona, Spain
[c] Departament de Ciència dels Materials i Enginyeria Metal·lúrgica, Universitat de Barcelona, Av Diagonal 647, E-08028 Barcelona, Spain

ARTICLE INFO

*Article history:*
Received 29 March 2011
Accepted 26 July 2011
Available online 5 August 2011

*Keywords:*
Fire protection material
Fire passive protection
Solid state kinetics
Endothermic degradation
Heat transfer
Gypsum

ABSTRACT

Passive Fire Protection is currently a field of active interest in building technology. One of the different approaches to obtain a material that provides this protection is to add substances to the initial formulation that are capable to absorb heat when the temperature of the material is increased. This is achieved by means of endothermic reactions that these substances undergo at specified temperatures. In the case of a fire scenario huge amounts of heat are released and such heat absorbing reactions delay the achievement of temperatures that can be critical for structural stability. In this work we specifically analyze the behavior of gypsum, which is commonly used in buildings. In order to enrich its endothermic profile we add magnesium hydroxide, calcium hydroxide and calcium carbonate to the sample. These three alkaline earth components have their heat absorbing peaks located along the temperature domain in a way that the temperature rising is reasonably damped. In this work we find, as the main result, that when these three fillers are added to gypsum, the protection offered by the new combination of materials is significantly improved with respect to the behavior of gypsum alone. Under external heating, the component is able to keep itself under critical temperatures for a longer period. For the theoretical description, we first use non isothermal thermogravimetry (TG) to analyze and characterize the kinetic response of each component of the mixture. We propose a conversion function which is based on the correlation between consecutive reactions in neighboring molecules. The heating rate is included in the model as an analytical variable. Later we perform high temperature tests in a tubular furnace and their corresponding numerical simulations where heat transfer is explicitly carried and mass transfer effects are discussed.



## 1. Introduction

Nowadays there is a growing interest in Fire Protection in building technology [1–5]. There are two main reasons. On the one hand, fire standards are becoming more restrictive. As a consequence, building materials have to be improved. On the other hand there is a higher social awareness of the risk of fire. This fact demands as well the use of materials that have a reasonably good behavior under a fire scenario.

There are two main approaches to fire protection: Active Fire Protection (AFP) and Passive Fire Protection (PFP). Their main goal is to fight and prevent a fire scenario. Specifically AFP consists in detecting signals of fire like smoke, flames or heat in order to activate premature extinction and evacuation, while PFP is focused on avoiding fire starting and damping its spreading minimizing the damages and guaranteeing the integrity of the structural elements [1,6–13] at least for an amount of time that guarantees evacuation [12].

In this work we focus our analysis into a specific PFP material. Protection of reinforced steel and concrete structures by means of fireproof mortars or plasters increase the fire resistance of the structural system. These fireproof materials are usually formed by a ceramic binder like Portland cement or gypsum and mineral fillers or aggregates. Specifically we will make use of a gypsum panel which has a pair of endothermic reactions around 100–150 °C. To this core material we will add three pure alkaline earth components: $Mg(OH)_2$ (magnesium hydroxide), $Ca(OH)_2$ (calcium hydroxide) and $CaCO_3$ (calcium carbonate). Previous works [14–16] have shown the possibility of using industrial by-products containing these components for its use in PFP. However, for analysis

* Corresponding author. Tel.: +34 934011835.
*E-mail address:* aleix@fa.upc.edu (A. Ciudad).

1359-4311/$ – see front matter © 2011 Elsevier Ltd. All rights reserved.
doi:10.1016/j.applthermaleng.2011.07.048

convenience we use here only substances with high levels of purity. We have chosen these three substances following two criteria. On the one hand, each of these three substances undergoes a simple heat absorbing peak, which makes the theoretical analysis more simple and clear. On the other hand, the three endothermic peaks that we obtain are fairly well spread along the temperature domain in the interesting range of (300, 1000) °C. $Mg(OH)_2$, $Ca(OH)_2$ and $CaCO_3$ have their endothermic transitions around 350, 450 and 950 °C, respectively, although the actual values depend on different variables. Specifically they strongly depend on the heating rate value in such a way that higher values of the heating rate produce wider peaks and more displaced to higher temperatures. We will include this dependence in our analysis. In short, with gypsum and the three mentioned earth components we can obtain a formulation that cushions an external temperature rising with better results than a panel made of gypsum alone.

Our approach will consist in analyzing each pure substance, including gypsum, with thermogravimetry performed at different constant heating rates. From the results of these tests we will prepare and test different formulations in order to understand the protection effect for each filler when added to a gypsum sample. We also formulate a combined formulation with the three fillers in order to obtain a material that optimizes the passive protection under external conditions where temperatures are above critical values for structural integrity purposes. In addition, we characterize each substance with simple kinetic parameters in a theory that contains the heating rate as a variable. The analytical heating rate dependence provides a valuable information [17] since in spatially extended system the actual heating rate is non homogeneous and non uniform. We will compare the results of tubular furnace tests of middle sized samples with theoretical simulations.

## 2. Material and methods

The samples were prepared with an E-35 gypsum plaster from Saint-Gobain Placo Iberica S.A. Magnesium hydroxide, calcium hydroxide and calcium carbonate analytical grades supplied by Panreac were chosen as endothermic fillers due to their endothermic decompositions with associated reaction heats of 1.37, 1.42 and 1.74 kJ/g, respectively [1819]. For the heat of reaction of gypsum we performed Differential Scanning Calorimetry in a DSC-822e/400 Mettler Toledo. The heating rate was set at 5 °C/min and the atmosphere was air. We obtained a value of 0.575 kJ/g.

The thermogravimetric analysis (TGA) was performed using a TGA-DTA 851e/SF/1100 from Mettler Toledo. The essays covered a temperature domain of (30,1000) °C in air atmosphere with four different heating rates from 2 °C/min to 50 °C/min.

In order to evaluate the behavior of spatially extended samples at high temperatures, the vertical furnace shown in Fig. 1, designed according to standard ISO 1182: Non-Combustibility Test, was used [20,21].

This device provided a cylindrical space with a 75 mm diameter and a 150 mm height where the specimen was placed. The temperature inside the furnace was measured by a thermocouple positioned at mid-height and at 10 mm from the wall. The sample had a cylindrical shape, with diameter 41 mm and height $h = 50$ mm. When the sample was being prepared and the mixture was still fresh, a thermocouple was introduced through the symmetry axis in a way that the tip of the thermocouple was located at the geometric center of the cylinder. In addition there was a third thermocouple, in contact with the surface of the specimen, diametrically opposed to the furnace thermocouple. All the thermocouples were of type K. The furnace and the surface thermocouples were protected with a stainless steel armor. Test samples were prepared and dried at 50 °C for one day. During the test, furnace temperature was increased at constant rate with electronic control, from room temperature to 800 °C in 2 h, and then remained at 800 °C for 60 additional minutes. The temperatures on the surface and center of the sample were recorded every 10 s.

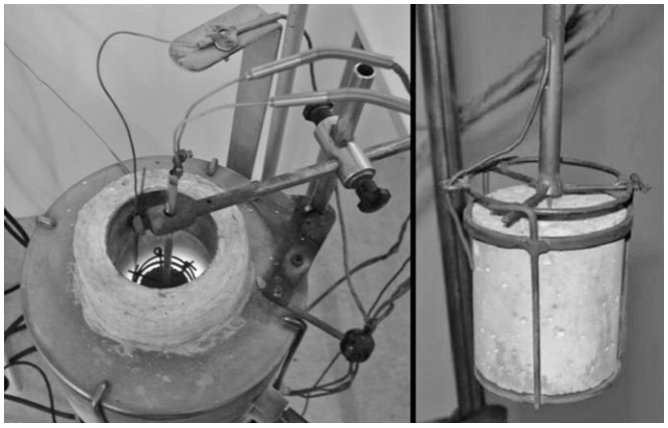

**Fig. 1.** On the left side of the image we can see the non-combustibility furnace at work with a sample inside. At real experiments the top is covered in order to avoid a significant heat flow in the vertical direction. On the right side we show a detail of a tested sample.

We prepared three different sample formulation, which we call Y1, Y2 and Y3 (See Table 1). Such diversity was due to the fact that magnesium and calcium hydroxides have their endothermic peaks at similar temperatures, which produces an overlapping in the heat absorbing process. Thus Y3 formulation contains the four substances, gypsum, $Mg(OH)_2$, $Ca(OH)_2$ and $CaCO_3$. Y1 sample lacks calcium hydroxide and Y2 does not include magnesium hydroxide. The idea of preparing Y1 and Y2 was observing the behavior of magnesium and calcium hydroxide independently, while Y3 was the target formulation in order to optimize the richness of the heat absorbing profile.

The choice of the specific formulation was not arbitrary. As our main goal was to achieve an optimal Fire Passive Protection we wanted to equalize the effect of the four endothermic reactions taking place during the heating process. However not each material has the same heat of reaction. What we did was to weigh each relative proportion with the weight of its heat of reaction in such a way that the amount of absorbed heat in the four substances was approximately the same. As said before, while Y3 sample has the four substances, Y1 and Y2 samples lack one of the components. Our choice was to fill the mass of the missing component with calcium carbonate. As a consequence, Y1 and Y2 do not have well balanced peaks but they keep the same total sample mass which is also a desirable condition in order to improve the reproducibility of the results. In Table 1 we show the resulting formulation of each type of sample. The proportions are shown for the initial preparation. We show in the last column the values of $\beta$, which is the proportion between the water mass after the drying process and the water mass just after the mixture was prepared.

In addition to the cylindrical samples, two rectangular samples with Y1 and Y2 formulations were prepared in order to determine

**Table 1**
Percentile proportions of gypsum (E−35) powder, magnesium hydroxide, calcium hydroxide and calcium carbonate in the three sample configurations Y1, Y2 and Y3.

| Sample | gypsum | $Mg(OH)_2$ | $Ca(OH)_2$ | $CaCO_3$ | $H_2O$ | $\beta$ |
|---|---|---|---|---|---|---|
| Y1 | 23.4 | 11.4 | 0.0 | 20.0 | 45.2 | 0.057 |
| Y2 | 24.0 | 0.0 | 11.3 | 21.1 | 43.6 | 0.117 |
| Y3 | 21.3 | 10.4 | 10.1 | 8.2 | 50.0 | 0.092 |

their thermal parameters. Thermal conductivity $\lambda$ and thermal diffusivity $\alpha$ were measured by a transient line-source technique with an Anter Quicktime™-30 instrument. Density $\rho$ was also measured in order to calculate the sensible specific heat $c_e = \lambda(\alpha\rho)$. In order to obtain values of $c_e$ and $\alpha$ at different temperatures we slowly heated the sample until it reached the desired temperature. We maintained the sample at this temperature for 4 h and then we slowly cooled it to room temperature again in order to proceed with the measure. When the analyzer completed the test we repeated the same heating/cooling protocol in order to reach the next temperature, which was always higher than the previous. The lateral dimensions of the samples were chosen in order to excess the probe surface. The depth was relevant to ensure a stable measurement. Several calibrations revealed that depths below 2 cm did not give correct values. Thus we built 15 × 15 × 2.5 $cm^3$ samples. The room temperature was 20 °C. The temperatures at which we heated the samples were, by increasing order, 20,75,110,150,200,300,430 and 550 °C. These values were chosen in a way that we could measure $c_e$ and $\alpha$ at the most relevant points of the endothermic profile, except for the calcium carbonate degradation regime which has a temperature at which the sample loses its integrity. With a fragmented sample the conductivity analyzer could not measure proper values.

Additionally, a Y1 sample was tested on a high temperature furnace capable of reaching temperatures beyond 1000 °C.

## 3. Theory

### 3.1. Kinetics

The kinetic approach to a solid state reaction has been widely explored in the literature, specially in the attempt to describe the degradation of calcium carbonate [22,23,25]. Many different techniques and models can be applied to fit the thermogravimetric data [26] but none of them will provide the real kinetic parameters. As discussed in [27] the reality of these parameters can be put into question. The best we can get is a set of parameters that fits our data for our specific experimental conditions. The mass loss as a function of time will not only depend on the heating rate but also on the mass sample, the inert gas flow, the type of inert gas, the specific analyzer or the concentration of the gaseous product [27,28].

For a detailed kinetic analysis an isoconversional method is usually applied [26,29]. This will provide the information of whether the reaction is a single step mechanism or not. However, such a detailed description of the kinetics of the endothermic transitions considered in this work is not our main point. We focus instead on describing at first order the endothermic transitions in order to analyze whether the results that fit the data for very low mass samples are useful to describe the endothermic profile of a much bigger spatially extended system. Thus it is enough to consider each reaction, even the double transition of gypsum, as a single step reaction.

There are several kinetic models for a single step reaction, depending on which conversion function f($x$) is used [26,29]. The general model is written as

$$\frac{dx}{dT} = Af(x)e^{-E/k_BT}, \tag{1}$$

where $x$ is the mass fraction that has already reacted, $A$ the pre-exponential factor, $E$ the activation barrier, $T$ the temperature and $k_B$ the Boltzmann constant. In this work we use a conversion function that is discussed in detail somewhere else [30]. It is based on the hypothesis that after a single molecule has undergone the endothermic reaction there is an effective number $N_c$ of surrounding molecules that cannot immediately react because the local thermal energy has been lowered due to the heat absorption. We thus call $N_c$ the correlation parameter, as it is a measure of how a reaction negatively correlates the reaction of the surrounding molecules. Notice that $N_c$ is not the same of the order of reaction $n$ which is widely used in several models. While for the limit where all chemical reactions are statistically independent and uncorrelated we have $N_c = n = 1$, for negatively correlated or anti-cooperative reactions we have $N_c > 1$ and $0 \le n < 1$.

The kinetic equation can be written as

$$\frac{dx}{dT} = \frac{\kappa A}{\phi N_c}e^{-E/k_BT}\left(1 - x^{N_c}\right), \tag{2}$$

where $\varphi$ is the heating rate, $\kappa = m_0/(m_0 - m_f)$ and $m_0$, $m_f$ are the initial and final masses of the sample in the TG test, respectively. This conversion function has the advantage that for a given $N_c > 1$, the quantity $(1 - x^{N_c})$ remains very close to unity for a considerable fraction of the test. While this approximation holds, the kinetics can be considered as independent of $x$ and the differential equation can be easily solved. Cropping the data within the domain where the approximation is valid we can obtain a fit for $E$ and the ratio $A/N_c$. After this process is completed we use the data not only from the initial stage of the mass decay but from the whole evolution in order to fit $N_c$ and obtain the value of A as well. The whole process is repeated on each test, each of one performed at a different heating rate. For each fit the values of the parameters are consistent but not exactly equal. We perform the average of the obtained values for the activation barrier $E$ and perform the whole fit process again now keeping the average $E$ as a fixed value. The resulting values for $A$ and $N_c$ are, after the second fit, much more convergent. We keep the average values of $A$ and $N_c$ from the different tests, weighting each curve depending on whether the mass of the sample is closer or further from 5 mg. The more distant the mass of the sample is from 5 mg the less it weights on the average. The reason for this is that the mass sample is a variable that dramatically affects the results. The greater the mass the more displaced is the endothermic peak to higher temperatures. In fact, the effect of a greater mass sample is quite resemblant to the effect of higher heating rates. A possible explanation is that with a greater mass there is an increasing spatially extended system effect where a considerable internal temperature gradient is produced but not measured. This is an important point that will play a role when applying the kinetic parameters from thermogravimetry to a much bigger sample in tubular furnace tests.

### 3.2. Spatially extended simulations

In a spatially extended system we cannot consider, as we do in 5 mg thermogravimetry samples, that the system is isothermal. Thus a detailed description of heat transfer and a position dependent temperature is needed. The mass transfer effects, at first order of approximation, can be neglected if we consider that the evacuation of products is fast enough. We will also consider that our samples are homogeneous. With these two hypothesis we can write the following equation for temperature $T$ as a function of time and position $\vec{r}(x,y,z)$,

$$c_p\rho\frac{\partial T(r,t)}{\partial t} = \lambda\left(\frac{\partial^2 T}{\partial x^2} + \frac{\partial^2 T}{\partial y^2} + \frac{\partial^2 T}{\partial z^2}\right), \tag{3}$$

where $\vec{r}(x,y,z)$ is the position vector as a function of Cartesian coordinates, $t$ is time and $c_p$ the apparent specific heat. The three magnitudes $c_p$, $\rho$ and $\lambda$ depend on temperature. As stated in the previous section we measure them at different temperatures in

order to obtain an interpolated expression for the dependence on temperature that can be used to numerically integrate the equation for $T(x, y, z, t)$.

The apparent specific heat is the sum of the intrinsic or sensible specific heat of the material and the heat of reaction of the endothermic transition,

$$c_p(T) = c_e(T) + \int_{T_1}^{T} \left( \sum_{i=1}^{4} \Delta H_i \xi_i \frac{dx_i}{dT} \right) dT, \quad (4)$$

where index $i$ runs for the four components of the system and $T_1$ is the initial temperature. $\Delta H_i$, $\xi_i$ and $dx_i$ are the heat of reaction, weight percentage and mass fraction of the $i$ component, respectively. In our samples we have a mixture of gypsum with the three alkaline earth components mentioned above. At first order we can consider that four endothermic reactions will take place along the whole temperature domain. Thus the apparent specific heat will have four peaks that correspond to each of the individual reactions.

As our samples have cylindrical symmetry (see Fig. 1), we use cylindrical coordinates and focus on the radial dependence. Thus equation [3] can be rewritten as

$$\frac{\partial T(r,t)}{\partial t} = \alpha \frac{c_e}{c_p} \left( \frac{\partial^2 T}{\partial r^2} + \frac{1}{r} \frac{\partial T}{\partial r} \right) \quad (5)$$

where $r$ is the radius and $c_e/c_p$ is a dimensionless magnitude. These two quantities, $c_e/c_p$ and $\alpha$, are the only magnitudes to which the temperature dependence needs to be established in order to numerically integrate equation [5].

The numerical integration of equation [5] is performed using a custom program. We define a lattice of 41 cells where each cell has a size of 0.0005 m. The time step is $\Delta t = 0.01$s, which is fine enough to use Euler's method. The boundary condition is imposed by the furnace temperature, which defines the external temperature as

$$T(r = R, t) = T_s(t) \quad (6)$$

where $R$ ($\simeq$2 cm) is the radius of the sample and $T_s$(t) is the time-dependent temperature of the sample surface imposed by the ramp programmed to the furnace controller. As the input for $T_s$(t) evolution we use the actual measured data from the thermocouple located at the surface of the sample.

Through the numerical integration process, the local and instantaneous value of the heating rate is computed in order to apply the most appropriate kinetic rate at each cell and at each time step. In order to see the possible effect of numerical fluctuations of $\phi$ we compare the results of using instantaneous values with a smoothed heating rate achieved by averaging the values of $\phi$ from the last 15 s. The discrepancies between the two methods are not significant.

## 4. Results

In Table 2 we show the obtained values for the kinetic parameters involved in equation [2]. We give the activation barrier $E$, the pre-exponential factor A and the correlation coefficient $N_c$. In the last column we also specify $\kappa$. This parameter can be calculated from the simplified chemical reaction or directly measured from the TG data. Both methods give the same results.

The values for $E$ and $A$, which are common to other conversion functions, are consistent with the values given in other works [24]. The activation barrier for gypsum has the lowest value while calcium carbonate exhibits the greatest value. As expected, both magnesium and calcium hydroxides have similar activation barrier values. In fact, the fitted value for calcium hydroxide seems to be lower than the corresponding barrier for magnesium hydroxide, even though the peak of the latter component appears first. This fact can be explained by the very different values that the two hydroxides exhibit in the pre-exponential factor. For magnesium hydroxide is five orders of magnitude greater than the value for calcium hydroxide. This big difference in A makes the peak of magnesium hydroxide to appear first in the heat absorbing profile. We recall here that the solutions of the fit process are not unique. Different sets of values can lead to very similar results. The values of $\kappa$ obtained from direct mass measurement are strongly consistent with the prediction given by the stoichiometry of the reaction.

**Table 2**
Results for the fit of the kinetic model for gypsum, magnesium hydroxide, calcium hydroxide and calcium carbonate.

| Substance | E (J) | A ($s^{-1}$) | $N_c$ | $\kappa$ |
|---|---|---|---|---|
| Gypsum | $1.73 \times 10^{-19}$ | $8.5\ 10^{10}$ | 1 | 4.59 |
| $Mg(OH)_2$ | $2.95 \times 10^{-19}$ | $1.3\ 10^{11}$ | 2 | 3.64 |
| $Ca(OH)_2$ | $2.20 \times 10^{-19}$ | $3.6\ 10^{6}$ | 5 | 4.11 |
| $CaCO_3$ | $3.24 \times 10^{-19}$ | $4.0\ 10^{6}$ | 5 | 2.27 |

The values for the correlation parameter $N_c$ are all consistent with the heats of reaction of each component, although not linearly. For greater heats of reaction it is expected that the negative correlation between the reaction of a molecule and the simultaneous reaction of the surrounding molecules is reinforced, thus giving a greater value of $N_c$. While for the gypsum, which has a heat of reaction of 0.575 kJ/g, $N_c$ is approximately equal to 1, in the case of calcium carbonate, which has a heat of reaction of 1.74 kJ/g, $N_c$ is approximately equal to 5. For the sake of simplicity we have kept integer values of $N_c$ recalling the intrinsic meaning of $N_c$, but a more refined fit gives non-integer values of the correlating parameter and then for calcium carbonate we obtain slightly greater values than for calcium hydroxide. However the improvement on the fit is not very significant for a first order approach. What is a significant aspect of $N_c$ is that the greater the correlation parameter the more asymmetric is the endothermic peak. Peaks for gypsum and magnesium are symmetric while the calcium carbonate peak is the most asymmetric. Thus asymmetry of the peaks is correlated with $N_c$.

In Fig. 2 we show the experimental peaks for the thermogravimetry tests of gypsum and the three alkaline earth components in comparison with the theoretical predictions based on the fitting process described above. The data from gypsum is shown at

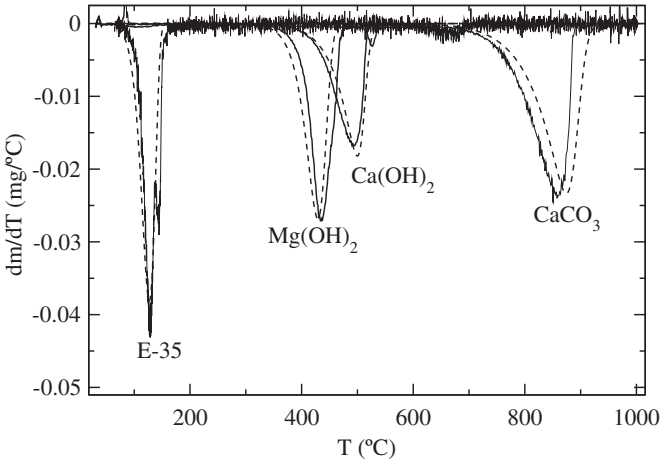


**Fig. 2.** Experimental TG data (solid lines) and theoretical predictions (dashed lines) for the four materials considered in our system: gypsum, magnesium hydroxide, calcium hydroxide and calcium carbonate.

a tested heating rate of 8 °C/min while the other three peaks correspond to $\phi = 50$ °C/min tests. Notice that gypsum gives a double peak that in our model is considered as a single reaction for the sake of simplicity. The figure explicitly shows how the temperature domain is covered by four endothermic transitions. The two hydroxides overlap in temperature, a fact that introduces some difficulties explained further in the text. The peak of calcium carbonate occurs at very high temperature and the tubular furnace will not reach this quantity. As temperature increases we can appreciate as well how the asymmetry of the peaks increases, in accordance with the increasing heat of reaction of the components. It is important to recall that while the match between theoretical curves and experimental data is not extremely accurate, we obtain a compromise of parameters that allow us to predict the behavior of theses substances at very different heating rates with the same degree of accuracy. We recall that the vertical axis shows the temperature derivative of the mass. This quantity is proportional to $dx/dT$ from equation [2]. More specifically, $x=(m - m_0)/(m_0 - m_f)$.

In Fig. 3 we show the results of thermogravimetric tests for calcium hydroxide at four different heating rates $\phi = 4$, 16, 25 and 50° C/min. We observe that for the $\phi = 4$, 25, 50 °C/min cases the mass of the sample is very similar, while for the $\phi = 16$ °C/min case it is a bit larger. For equal masses the tendency of the TG evolution is to develop wider peaks and more displaced to higher temperatures as the heating rate is increased. However, the effect of the mass, which is not explicitly incorporated in our model, also modifies the mass evolution displacing the peaks to higher temperatures as the mass increases. During the fit process the $\phi = 16$ °C/min case has less statistical weight that the other three cases. The asymmetry of the peaks is manifest by the long branch at lower temperatures and the steepness at higher temperatures. We show the mass of the sample in each case, which allows us to observe that for higher masses the peak becomes deeper when plotted as the derivative of the mass with respect to the temperature. When plotted using the derivative of the mass fraction with respect to the temperature the effect of a larger mass is very similar to the effect of a higher heating rate, i.e. the peak is displaced to higher temperatures and becomes wider. On the other hand, the dependence of the transition shape on the heating rate is very systematic. Higher heating rates move the peaks to higher temperatures. The peaks also become wider and their height is also reduced.

The results of the measurements for the sensible specific heat are shown in Fig. 4. We recall that all values are measured at room temperature after bringing the sample for some hours at the temperature indicated in the horizontal axis. We have performed tests for the Y1 and Y2 formulations obtaining results with similar behavior. In both formulations the specific heat remains constant until the endothermic reaction undergone by the gypsum takes place and its value drops abruptly. The new value of $c_e$ remains approximately constant until the two hydroxides start to degrade, which has the effect of increasing the specific heat to a new value which is greater than the later but lower than the initial value at room temperature. The difference between the formulations Y1 and Y2 is that the former undergoes a deeper drop of $c_e$ after gypsum dehydration. Additionally we assume the behavior of formulation Y3 to be a middle way between the evolution of Y1 and Y2. For values greater than 600 °C we have no reliable measurements as the samples become systematically cracked. We consider that beyond this temperature $c_e$ remains constant even though we think that calcium carbonate degradation may have an effect on this magnitude. The data is approximated by a piece wise function. Small variations in this function do not have a strong effect on the simulations.

The results for the diffusivity $\alpha$ as a function of temperature are shown in Fig. 5 and are strongly correlated with the results for $c_e$ as $\alpha$ is in fact a function of the specific heat. By this we mean that the changes of values occur at similar temperatures. However $\alpha$ is also a function of density and thermal conductivity, which makes the evolution of $\alpha$ distinctively significant. The values of $\alpha$ are approximately constant until gypsum dehydration begins, which produces an increase which is similar between formulations Y1 and Y2. This is different from what happens with $c_e$, where its value dropped differently for Y1 and Y2. When the hydroxide reactions start the diffusivity increases again. Such increase is different between Y1 and Y2, being the change in Y2 more pronounced. Again we consider in this last regime that the evolution of Y3 will be a middle way between Y1 and Y2. Notice that while $c_e$ first dropped and later increased again, the evolution of $\alpha$ is ascendant during the two transitions. For values greater than 600*o* we again consider that the function remains constant. The justification of this hypothesis and the difficulties of measuring values on greater temperatures are the same as mentioned before for $c_e$ analysis.

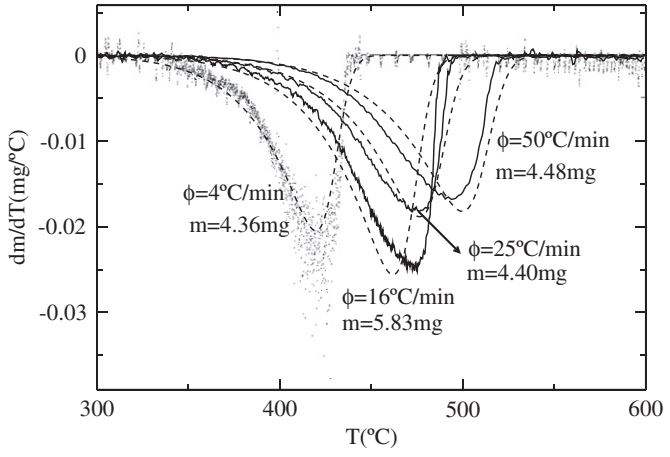


**Fig. 3.** Temperature derivative of the mass ($dm/dT$) plotted versus the temperature $T$ for calcium hydroxide samples under thermogravimetric analysis. We show the results for 4 different heating rates of values $\phi = 4$,16,25,50 °C/min. The masses of the samples are 4.36, 5.83, 4.40 and 4.48 mg respectively. In the $\phi = 4$ °C/min case experimental data is plotted in small dots, while the other three cases is plotted in solid line. Theoretical predictions are shown in dashed lines.

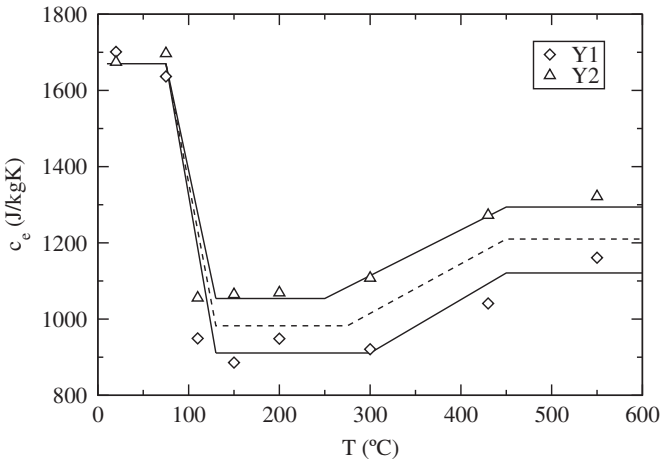


**Fig. 4.** Sensible specific heat plotted versus temperature. Points are experimental. Lines are fits. Diamonds show data for the Y1 sample while up triangles show data for Y2 sample. For Y1 and Y2 solid lines are used in the fit. The dashed line represents and average between the two solid lines. We use this average for the behavior of the Y3 sample.

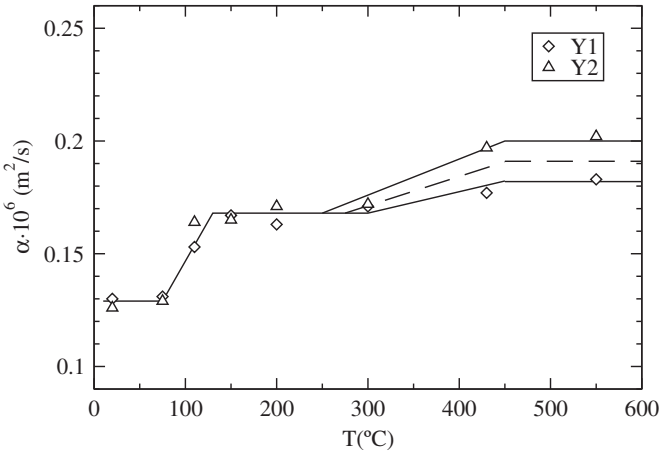


**Fig. 5.** Thermal diffusivity plotted versus temperature. As in Fig. 4, points are experimental and lines are numerical fits. Diamonds and up triangles show data for Y1 and Y2 samples, respectively. Solid lines are fits for Y1 and Y2 while the dashed line is the average behavior between them, which we use as the input for the Y3 sample.

In Fig. 6 we show the results for the tubular furnace test using a sample with Y1 formulation, i.e. where no calcium hydroxide has been added. We appreciate an initial plateau corresponding to gypsum dehydration and a second plateau that is the signal for the decomposition of magnesium hydroxide. The final plateau only means that the sample has reached thermal equilibrium with the final state of the furnace at 700 °C. We also plot the result of the numerical integration of equation [5] with the corresponding kinetic parameters and with the experimental boundary conditions given by the furnace ramp. We appreciate that the agreement is reasonable, even though in the simulations the plateaus at the endothermic reactions tend to last longer. Moreover we notice that the furnace does not arrive to the calcium carbonate degradation regime, so we only observe the gypsum and the magnesium hydroxide reactions. The last plateau at approximately 700 °C corresponds to the final temperature of the furnace.

However, in order to obtain the curve shown in the figure we have to multiply the value of the activation barrier in the kinetic equations by a constant factor we call $\varepsilon$. If we do not perform this operation the agreement that shows the figure cannot be achieved.

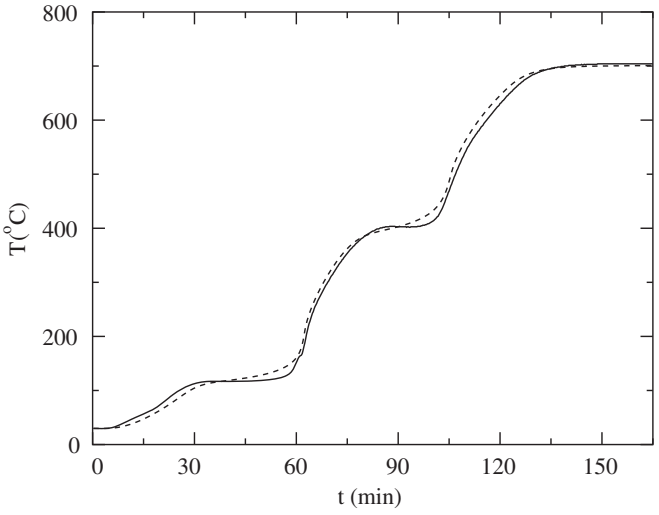


**Fig. 6.** Temperature plotted versus time for a tubular furnace test for the Y1 sample, which does not contain calcium hydroxide. Solid line shows the experimental data and dashed line the result of the numerical simulation for $\varepsilon = 1.1$.

Different values of this multiplicative constant have been tested and all the results shown from now on have a value of $\varepsilon = 1.1$. The need for the introduction of $\varepsilon$ and its significance is discussed in next section.

The results of the tubular furnace test for the Y2 sample and its corresponding numerical simulation are shown in Fig. 7. The same phenomenology discussed for Fig. 6 holds here as well. The only change is that in Y2 we have no magnesium hydroxide and we do have calcium hydroxide instead. The plateau due to the hydroxide transition is less flat than in magnesium hydroxide. This fact may be related with the difference of the thermogravimetric peaks between endothermic transitions for magnesium and calcium hydroxide. The former exhibits a narrower peak than the latter (see Fig. 2). Consequently, the magnesium hydroxide degradation occurs at a more restricted temperature window than in the case of calcium hydroxide, thus showing a flatter plateau. The agreement between theory and experimental data is better for the Y1 formulation but we still have a reasonable match between the two curves. If we compare this figure with Fig. 6 we can see how the reactions for the two hydroxides widely overlap, even though the reaction for the calcium hydroxide begins at slightly greater temperature.

The Y3 formulation contains both magnesium and calcium hydroxide and their degradation occurs in overlapping regimes. This fact can be observed in Fig. 8, where we have also included the result of the numerical simulation. We see that the theory predicts a strong overlapping between the two hydroxide degradations. The experiment actually shows that there is an overlapping, but less pronounced than the theoretical prediction. In this case the temperature interval between 400 °C and 700 °C, which corresponds to the two overlapped hydroxide reactions, does not exhibit such a good agreement as in the previous cases where only one hydroxide was present. We can see that the plateau corresponding to the degradation of gypsum is longer. This is due to the greater amount of gypsum in this sample. Notice how fast the sample temperature ascends after the transition to follow the same evolution that the furnace from time $t \simeq 90$ min.

Finally, as the calcium carbonate degradation regime cannot be reached by the tubular furnace, we test a Y1 sample on a high temperature furnace. We show the results in Fig. 9. In this case we use another furnace which is more rudimentary and has not a cylindrical shape, unlike the tubular furnace used in the rest of the

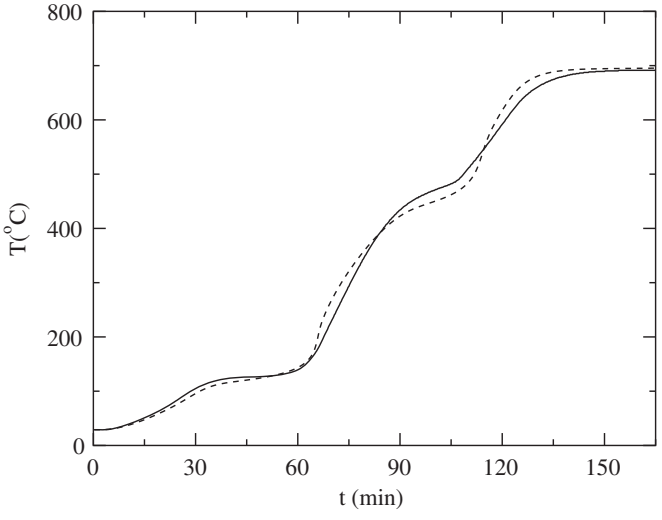


**Fig. 7.** Temperature plotted versus time for a tubular furnace test for the Y2 sample, which does not contain magnesium hydroxide. In a similar way as in Fig. 6 we use solid line for experimental data and dashed line for the simulation results with $\varepsilon = 1.1$ for all the components.

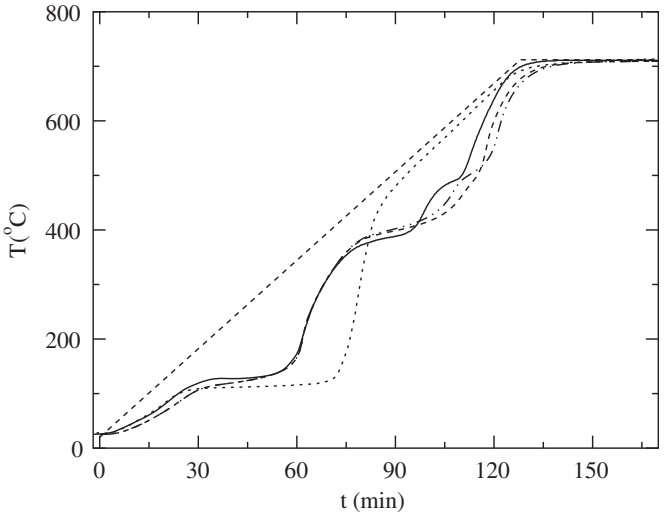


**Fig. 8.** Temperature plotted versus time for a tubular furnace test for the Y3 sample, which contains both magnesium and calcium hydroxide. As in Figs. 6 and 7 we use solid line for experimental data. The dotted line shows the evolution of a sample entirely made by gypsum tested under the same furnace protocol. The dot-dash line shows the furnace ramp imposed on the external surface of the sample. Additionally, the dashed line shows the numerical results for $\varepsilon = 1.1$ while the dot-dot-dash line shows the result of a simulation where we set $\varepsilon = 1.1$ for all components except for calcium hydroxide, where we set $\varepsilon = 1.15$.

tests. However in the current test we can reach higher temperatures which allows to observe the transition due to the calcium carbonate degradation. The four plateaus corresponding to the four components of the Y1 formulation can be clearly observed. The non-cylindrical symmetry of the furnace does not allow the use of equation [5] to simulate this system, so we only show the experimental curve.

## 5. Discussion

The thermogravimetric tests have allowed us to extract kinetic information from the mass variations of the sample. We have used this information to describe the heat absorbing behavior assuming that both mass and heat variations have to be proportional to the underlying kinetics. Moreover, the multi-factorial dependence of the kinetic parameters show that the fitted values do not have an absolute meaning beyond the specific experimental setup. However, in order to characterize the heat transfer properties of a relatively big sample it is important to know the kinetic properties of its components, at least at first order of accuracy. But this kinetic information needs to be extracted from tests performed on samples with small masses [31] in order to avoid significant thermal gradients on the system. As a consequence, the need for an extrapolation when the scale of the setup is changed is manifest. In this work we have found that there is a considerable discrepancy between the kinetic behavior in a small sample at a given rate and the local kinetic behavior of each small portion of the medium size sample when computing its local and instantaneous heating rate. Specifically we find that the kinetic evolution in the cylindrical samples at a given heating rate corresponds to a small 5 mg sample with an activation barrier 1.1 times bigger. In other words, with bigger samples the endothermic peaks behave like having greater activation barriers. The reason of this behavior can be explained by means of mass transport, which is not directly included in our model. Whenever gypsum decomposition is completed a considerable amount of water escapes from the sample. If water loss is fast there is no reason to expect a displacement in the activation barrier of the gypsum or subsequent decomposition reactions. However, such a displacement is observed. This is the reason why we introduce the multiplier $\varepsilon$ in the activation barrier. The presence of temporarily trapped water in the sample displaces the gypsum reactions to greater temperatures, and the same effect is observed in the decomposition of magnesium hydroxide, which also has water as a product. Additionally, the water produced by the latter reaction affects the appearance of the calcium hydroxide decomposition. In short, the evacuation of water seems to be slow enough to delay the course of each reaction and the appearance of the next peak. In Fig. 8 we show the results for $\varepsilon = 1.1$ for all components in a dashed line. However, we see that if we increase $\varepsilon$ to 1.15 only for calcium hydroxide (dot-dot-dash line) the agreement is improved. This suggests that the degradation of calcium hydroxide is more affected by the presence of water due to the proximity of the previous decomposition of magnesium hydroxide. For calcium carbonate we do not expect water to significantly affect its degradation as it is not a product. However, the transport of the produced $CO_2$ may displace the peak if the sample does not become very fragmented.

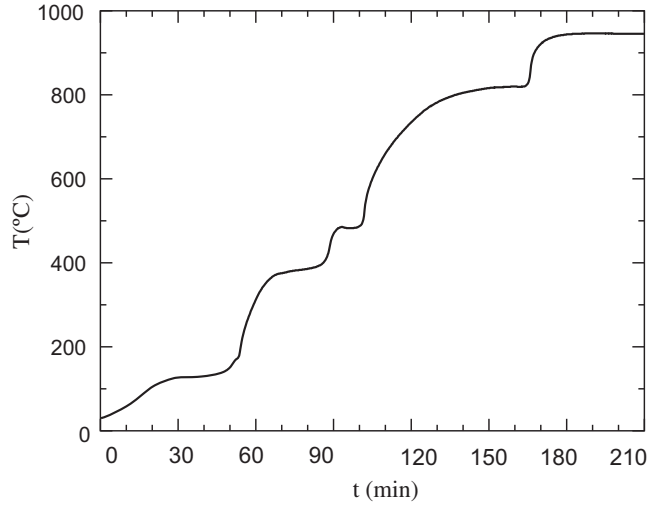


**Fig. 9.** Temperature plotted versus time for a furnace test for the Y3 sample, which contains both magnesium and calcium hydroxide.

To change the value for the activation barrier $E$ alone is not the most rigorous action to incorporate the presence of significant amounts of product in the reaction. However, by this simple and effective transformation we are able to reproduce the main tendency of the peak shift, although we may lose information from the specific peak shape. Future work has to focus on describing explicitly the mass transport which may depend on the porosity, the inhomogeneities and other complex features of the sample. Additionally, the kinetic description will have to take into account the presence of products that are able to modify its rates and what is more important, to couple the different reactions.

The coupling between consecutive reactions is manifest in our results. Tubular furnace data show a clear separation between the magnesium and the calcium carbonate peaks, as seen in Figs. 8 and 9. Simulations predict that these peaks should overlap. Although we have not shown thermogravimetric data for the whole formulation, several tests with both hydroxides have been performed showing that the clear separation between the two peaks is reproduced at small scales as well. This is explained again by the presence water in the sample which, being a product in both reactions, slows the completion of the current reaction and delays the appearance of the next peak.

From what we can observe in Fig. 8 the passive protection that we achieve is improved on the larger temperature regimes at the

**Table 3**
Comparative of the Passive Protection given by a simple gypsum panel and a Y3 formulation. What we measure is the time elapsed when each material arrives at a given temperature. We choose 100,200,400 and 500 °C as representative temperatures.

| $T$ (°C) | $t_{Y3}$ (min) | $t_G$ (min) |
|---|---|---|
| 100 | 24 | 24 |
| 200 | 61 | 76 |
| 400 | 95 | 82 |
| 500 | 110 | 93 |

cost of reducing the protection at lower temperatures. We can notice as well that even though an endothermic transition cushions the temperature raise for an amount of time, once the reaction is complete the gradient temperature significantly grows because the sample and the furnace are at more distant temperatures. This produces an acceleration in the temperature profile that rapidly compensates the temperature difference. From this point of view the benefits of passive fire protection, we see that having endothermic transitions in the formulation clearly permits the sample to be at lower temperatures during the transitions. However, the overall temperature increasing rate is not clearly diminished. We can quantify the level of protection by giving the time that a sample elapses until it reaches a given temperature. Let $t_G$ and $t_{Y3}$ be the times for a plain gypsum sample and a Y3 sample, respectively. In Table 3 we show the values of these times for four different temperatures. We see how even though the plain gypsum sample achieves a better protection for low temperatures, the Y3 formulation is clearly better for higher temperatures, where the main structural damage is made in a fire scenario. Concrete structures suffer a significant decrease in mechanical properties beyond 400 °C due to the dehydration of silicates and decomposition of portlandite. Furthermore, steel expands, softens and loses half of its mechanical strength around 550 °C. For this reason, we consider 400 and 550 °C as critical temperatures in structures when considering passive fire protection.

## 6. Conclusions

As a summary of concluding remarks we can say that this work presents a Passive Fire Protection formulation that exhibits a broad heat absorbing profile in the temperature domain from room temperature up to 1000 °C. Using three alkaline earth components we are able to distribute four endothermic transitions along this domain. The main result is that the presence of the three fillers clearly improves the protection given by the material when compared with the protection offered by gypsum alone. Then, from the point of view of Fire Protection, the use of simple gypsum panels could be substituted by our improved formulation. This is a significant result and it would allow building walls to keep its internal temperature below critical values for longer times.

In addition to the experimental results, we characterize an effective single step kinetics on each pure component for its use in numerical simulations of the heat transfer through the spatial and temporal evolution of the temperature of the sample. However, we find that the numerical results match the experimental data only when the effective activation barrier included in the kinetic equation is increased. This motivates further work in the description of mass transport and how it couples different chemical reactions.

## Acknowledgements

This work was supported by the MICINN (Spain) under Projects No.FIS2009-13360 and No. P37/08, and by Generalitat de Catalunya under Project No. 2009SGR878.

## References

[1] D. Kontogeorgos, M. Founti, Numerical investigation of simultaneous heat and mass transfer mechanisms occurring in a gypsum board exposed to fire conditions, Applied Thermal Engineering 30 (2010) 1461–1469.
[2] L. Wullschleger, K.G. Wakili, Numerical parameter study of the thermal behaviour of a gypsum plaster board at fire temperatures, Fire and Materials 32 (2008) 103–119.
[3] D. Kontogeorgos, I. Mandilaras, M. Founti, Scrutinizing gypsum board thermal performance at dehydration temperatures, Journal of Fire Sciences 29 (2) (2011) 111–130.
[4] K.G. Wakili, E. Hugi, Four types of gypsum plaster boards and their thermophysical properties under fire condition, Journal of Fire Sciences 27 (1) (2009) 27–43.
[5] S.V. Shepel, K.G. Wakili, E. Hugi, Vapor convection in gypsum plasterboard exposed to fire: numerical simulation and validation, numerical heat transfer, Part A: Applications: An International Journal of Computation and Methodology 57 (12) (2010) 911–935.
[6] L.F. Vilches, C. Leiva, J. Vale, C. Fernandez-Pereira, Insulating capacity of fly ash pastes used for passive protection against fire, Cement and Concrete Composites 27 (2005) 776–781.
[7] J.R. Mehaffey, P. Cuerrier, G. Carisse, A model for predicting heat transfer through gypsum-board/wood-stud walls exposed to fire, Fire and Materials 18 (1994) 297–305.
[8] M.V. Borrachero, J. Payá, M. Bonilla, J. Monzó, The use of thermogravimetric analysis technique for the characterization of construction materials, Journal of Thermal Analysis and Calorimetry 91 (2) (2008) 503–509.
[9] C.N. Ang, Y.C. Wang, Effect of moisture transfer on specific heat of gypsum plasterboard at high temperatures, Construction and Building Materials 23 (2009) 675–686.
[10] G. Thomas, Thermal properties of gypsum plasterboard at high temperatures, Fire and Materials 26 (2002) 37–45.
[11] H.E. Kissinger, Reaction kinetics in differential thermal analysis, Analytical Chemistry 29 (11) (1957) 1702–1706.
[12] D. Mai, Cement-Based Mineral-Containing Passive Fire Protection for Underground Structures, Fourth International Symposium on Sprayed Concrete (2002).
[13] M.A. Sultan, A model for predicting heat transfer through noninsulated unloaded steel-stud gypsum board wall assemblies exposed to fire, Fire Technology 32 (3) (1996) 239–259.
[14] J. Formosa, J.M. Chimenos, A.M. Lacasta, L. Haurie, Thermal study of low-grade magnesium hydroxide used as fire retardant and in passive fire protection, Thermochimica Acta 515 (2011) 43–50.
[15] J. Formosa, J.M. Chimenos, A.M. Lacasta, L. Haurie, J.R. Rosell, Novel fire-protecting mortars formulated with magnesium by-products, Cement and Concrete Research 41 (2011) 191–196.
[16] J. Formosa, L. Haurie, J.M. Chimenos, A.M. Lacasta, J.R. Rosell, Comparative study of magnesium by-products and vermiculite formulations to obtain fire resistant mortars, Materials Science Forum 587-588 (2008) 898–902.
[17] H.E. Kissinger, Variation of peak temperature with heating rate in differential thermal analysis, Journal of Research of the National Bureau of Standars 57 (1956) 4.
[18] W. Sha, G.B. Pereira, Differential scanning calorimetry study of hydrated ground granulated blast-furnace slag, Cement and Concrete Research 31 (2001) 327–329.
[19] P.A. Larcey, J.P. Redfern, G.M. Bell, Studies on magnesium hydroxide in polypropylene using simultaneous TG-DSC, Fire and Materials 19 (1995) 283–285.
[20] ASTM E136-09 Standard Test Method for Behavior of Materials in a Vertical Tube Furnace at 750°C.
[21] ISO 1182, Reaction to fire tests for building products:Non-combustibility test (2002).
[22] J.P. Elder, Reconciliation of Arrhenius and iso-conversional analysis kinetics parameters of non-isothermal data, Thermochimica Acta 272 (272) (1996) 41–48.
[23] M.E. Brown, M. Maciejewski, S. Vyazovkin, R. Nomen, J. Sempere, A. Burnham, J. Opfermann, R. Strey, H.L. Anderson, A. Kemmler, R. Keuleers, J. Janssens, H.O. Desseyn, Chao-Rui Li, Tong B. Tang, B. Roduit, J. Malek, T. Mitsuhashi, Computational aspects of kinetic analysis, Part A, Thermochimica Acta 355 (2000) 125–143.
[24] B. Roduit, Computational aspects of kinetic analysis, Part E, Thermochimica Acta 355 (2000) 171–180.
[25] C.F. Dickinson, G.R. Heal, A review of the ICTAC kinetics Project, 2000, Part 1. Thermochimica Acta 494 (2009) 1–14.
[26] S. Vyazovkin, Kinetic concepts of thermally stimulated reactions in solids: a view from a historical perspective, International Reviews. in Physical Chemistry 19 (1) (2000) 45–60.
[27] M. Maciejewski, Somewhere between fiction and reality, Journal of Thermal Analysis 38 (1992) 51–70.
[28] K. Ghazi Wakili, E. Hugi, L. Wullschleger, T. Frank, Gypsum board in fire modeling and experimental validation, Journal of Fire Sciences 25 (2007) 267–282.
[29] S. Vyazovkin, Handbook of Thermal Analysis and Calorimetry (Chapter 13), In: Isoconversional kinetics, vol. 5. Elsevier, 2008.
[30] A. Ciudad, L. Haurie, A.M. Lacasta, To appear in Journal of Thermal Analysis and Calorimetry in the special issue Medicta 2011.
[31] M.E. Brown, Introduction to Thermal Analysis. Kluwer Academic Publishers, 2001.